

Supercapacitor Sizing Method for Energy-Controlled Filter-Based Hybrid Energy Storage Systems

Damith Buddika Wickramasinghe Abeywardana, *Student Member, IEEE*, Branislav Hredzak, *Senior Member, IEEE*, Vassilios G. Agelidis, *Senior Member, IEEE*, and Georgios D. Demetriades, *Member, IEEE*

Abstract—Filter-based battery–supercapacitor hybrid energy storage systems (HESSs) are popular as a way of extending battery lifetime by diverging the high-frequency power variations to the supercapacitor. However, when a traditional supercapacitor voltage controller (SCVC) is employed in the filter-based HESS, precise sizing of the supercapacitor as well as finding filter parameters for the power allocation are challenging due to nonlinearities. These problems can be circumvented by using a supercapacitor energy controller (SCEC) proposed in this paper. The paper presents a method for selection of the SCEC and filter parameters as well as precise sizing of the supercapacitor for a given application. The proposed method is experimentally verified on a single-phase grid-connected HESS used to smooth the power delivered to the grid at the point of common coupling. It is also shown that the size of the supercapacitor when using the SCEC is significantly lower than the one estimated for the traditional SCVC.

Index Terms—Battery, hybrid energy storage system (HESS), supercapacitor, supercapacitor sizing.

NOMENCLATURE

HESS	Hybrid energy storage system.	L_{batt1}, L_{batt2}	Left-hand-side and right-hand-side battery connected inductors.
SoC	State of charge.	R_{Lbatt1}, R_{Lbatt2}	Equivalent series resistance of inductor L_{batt1} and L_{batt2} .
SCVC	Supercapacitor voltage controller.	i_{Lbatt1}, i_{Lbatt2}	Currents through inductors L_{batt1} and L_{batt2} .
SCEC	Supercapacitor energy controller.	C_1, C_2	Left-hand-side and right-hand-side output capacitors.
PV	Photovoltaic.	R_{C_1}, R_{C_2}	Equivalent series resistance of capacitors C_1 and C_2 .
HPF	High-pass filter.	v_{o1}, v_{o2}	Voltages across output capacitors C_1 and C_2 .
LiFePO ₄	Lithium iron phosphate.	i_{c1}, i_{c2}	Current through output capacitors C_1 and C_2 .
PR	Proportional resonant.	i_{o1}, i_{o2}	Output currents from left-hand-side and right-hand-side boost converter legs.
ESR	Equivalent series resistance.	i_g	Current supplied from the HESS to the grid.
v_{batt}, v_{sc}	Battery terminal voltage, supercapacitor terminal voltage.	L_g	Grid interfacing inductor.
i_{batt}, i_{sc}	Battery current, supercapacitor current.	V_o	HESS output voltage amplitude.
L_{sc1}, L_{sc2}	Left-hand-side and right-hand-side supercapacitor-connected inductors.	ω	Frequency of the HESS output voltage and grid voltage.
R_{Lsc1}, R_{Lsc2}	Equivalent series resistance of inductor L_{sc1} and L_{sc2} .	δ	HESS output voltage phase angle.
i_{Lsc1}, i_{Lsc2}	Currents through inductors L_{sc1} and L_{sc2} .	V_{dc}	DC shift of the output capacitor reference voltages.
		P_{HESS}	Output active power from the HESS.
		Q_{HESS}	Output reactive power from the HESS.
		P_{tot}	Total power supplied by the battery and the supercapacitor.
		P_{tot1}	Total input power supplied by the left-hand-side boost converter legs.
		P_{sc}	Total power supplied by the supercapacitor.
		P_{sc1}	Power supplied by the supercapacitor through the left-hand-side boost converter leg.
		P_{batt}	Total power supplied by the battery.
		P_{batt1}	Power supplied by the battery through the left-hand-side boost converter leg.
		$H_{HPF}(s)$	High-pass filter transfer function.
		a	Inverse value of the high-pass filter cut-off frequency.
		η	Efficiency of the HESS.
		C_{sc}	Capacitance of the supercapacitor.
		E_{sc}	Stored energy in the supercapacitor.
		$E_{sc,u}$	Utilized supercapacitor energy.
		$v_{sc,max}, v_{sc,min}$	Maximum and minimum supercapacitor voltage limits.
		$E_{sc,max}, E_{sc,min}$	Maximum and minimum supercapacitor energy limits.

Manuscript received July 7, 2015; revised November 16, 2015 and February 1, 2016; accepted April 2, 2016. Date of publication April 8, 2016; date of current version November 11, 2016. Recommended for publication by Associate Editor B. Semail.

D. B. W. Abeywardana, B. Hredzak, and V. G. Agelidis are with the School of Electrical Engineering and Telecommunications, Australian Energy Research Institute, The University of New South Wales, Sydney, NSW 2052, Australia (e-mail: d.wickramasingheabeywardana@student.unsw.edu.au; b.hredzak@unsw.edu.au; vassilios.agelidis@unsw.edu.au).

G. D. Demetriades is with the ABB Corporate Research, Västerås 721 78, Sweden (e-mail: georgios.demetriades@se.abb.com).

Color versions of one or more of the figures in this paper are available online at <http://ieeexplore.ieee.org>.

Digital Object Identifier 10.1109/TPEL.2016.2552198

dE_{sc}	Supercapacitor energy variation.
$K_{p,v_{sc}}, K_{p,Esc}$	Gain of SCVC, gain of SCEC.
$H_{Psc}(s)$	Transfer function between P_{sc} and P_{HESS} .
$H_{Pbatt}(s)$	Transfer function between P_{batt} and P_{HESS} .
$H_{dEsc}(s)$	Transfer function between d_{Esc} and P_{HESS} .
z_1, p_1, p_2	zero and poles of the transfer function H_{Pbatt} .
ω_c	Gain cross-over frequency of H_{Pbatt} .
P_{PV}	Power generated from the PV plant.
P_{grid}	Power injected to the grid.
$\nabla P_{tot}, \nabla P_{batt}$	Gradient of P_{tot} , gradient of P_{batt} .
$\nabla P_{batt.limit}$	Predefined maximum allowable gradient of the battery power profile P_{batt} .

I. INTRODUCTION

BATTERY-SUPERCAPACITOR hybrid energy storage systems (HESSs) have been proposed as a way of extending the battery lifetime and increasing the system power capability in many applications such as electric vehicles and grid energy storage [1]–[30]. In literature, it was shown that smoothness of the battery power profile has a significant impact on the battery lifetime [29]–[34], and hence, in battery-supercapacitor HESSs, fast power fluctuations are allocated to the supercapacitor.

Energy storage sizing is an important aspect of the HESS design. Numerous studies have been conducted to identify suitable energy storage sizing methods for battery-supercapacitor HESSs and the sizing methods are strongly coupled with the power allocation method [13]–[20], [25].

Among many power allocation methods proposed for the HESSs, the simplest possible power allocation strategy is the frequency-based power allocation where the high-frequency component of the total power requirement is allocated to the supercapacitor [2]–[4], [12]–[16], [23]–[25], [30]. In passive HESS, the power allocation frequency is determined by the impedance of the energy storage elements, while in active HESS, high-pass or low-pass filters are used to achieve the power allocation. Even though many power allocation methods were proposed for the HESSs using advanced control methods such as model predictive control [6], [7], fuzzy logic control [8], [9], and neural networks [10], [11], the filter-based power allocation provides a simple and effective approach to achieve the required performance. Energy storage sizing considerations reported in [15]–[20] were analyzed for non-filter-based power allocation strategies. Since the HESS sizing process is strongly dependent on the power allocation method, the before mentioned analysis methods are not applicable to the filter-based HESSs.

In the filter-based HESSs, the filter cut-off frequency determines the power components supplied by each energy storage element. The power allocation frequency can be determined based on the requirements of the HESS and once the power allocation frequency is determined, the required supercapacitor size can be identified to limit the supercapacitor operation within its maximum and minimum voltage limits [13], [14], [16], [25].

In [16], authors presented a HESS cost minimization method to select the power allocation frequency and the supercapacitor size. In [13] and [14], the HESS design was done based on the Ragone theory. A supercapacitor sizing method for an HESS with a pulsed power load was analyzed in [25]. However, in these papers, the supercapacitor state of charge (SoC) control was not considered.

In the HESSs, the supercapacitor voltage tends to fluctuate in a large range. Hence, the supercapacitor SoC control is vital to reduce the risk of supercapacitor overcharging or overdischarging [15], [35], [36]. By designing a proper supercapacitor SoC controller, the SoC can be maintained within a safe region.

As a way of supercapacitor SoC control, the supercapacitor voltage controllers (SCVCs) were employed in the filter-based HESS proposed in [2], [3], [21], and [30]. However, in these papers, the effect of the SCVC on the HESS power allocation or energy storage sizing was not analyzed. Due to nonlinearity of the SCVC, it is challenging to obtain simplified solutions for the power components supplied by each storage element. Moreover, the relationship between the total HESS output power and the power supplied by the supercapacitor depends on the supercapacitor size and, hence, cannot be used for accurate supercapacitor sizing. The effect of the supercapacitor SoC controller on the filter-based power allocation strategy is not analyzed in the current literature.

Analyzing the effect of the supercapacitor SoC controller on the HESS power allocation is vital: 1) to determine the high-pass filter and the supercapacitor SoC controller parameters required to obtain the desired HESS performance and 2) to determine the required energy storage sizes for a considered application.

In this paper, a supercapacitor sizing method and a HESS power allocation parameter selection method are studied for a supercapacitor SoC controlled, filter-based battery-supercapacitor HESS. First, the operation of the filter-based HESS with conventional SCVC is analyzed and the challenges posed by the SCVC on the supercapacitor sizing and HESS parameter selection are presented. Then, a supercapacitor energy controller (SCEC) is proposed for a high-pass filter-based HESS in order to alleviate the issues related to the nonlinearity of the SCVC. Effect of the SCEC on the filter-based HESS power allocation strategy is extensively analyzed. It is shown that the SCEC parameters have a significant effect on the power allocation frequency. A method to calculate the required high-pass filter and SCEC parameters along with the required supercapacitor size to meet specific HESS requirements is presented. The SCEC and its effects on the HESS performance are validated using both theoretical and experimental results.

The remainder of the paper is as follows. Section II describes the operation of the battery-supercapacitor HESS with the SCVC and later the proposed SCEC and its effects on HESS power allocation are extensively analyzed. The HESS power allocation parameter selection and supercapacitor sizing for a PV power smoothing application is studied in Section III. Section IV presents the experimental results to validate the operation of the HESS with SCEC while conclusions of the paper are summarized in Section V.

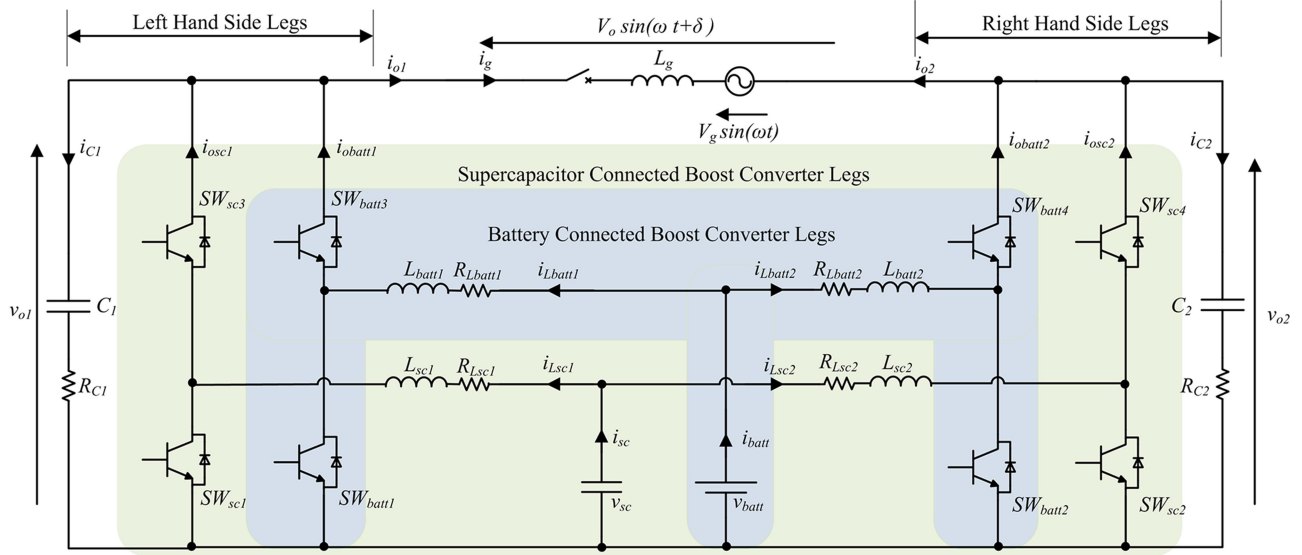


Fig. 1. Single-phase grid-connected battery–supercapacitor HESS.

II. HESS OPERATION WITH SCVC AND PROPOSED SCEC

In this section, first, the basic operation of a recently proposed boost inverter based battery–supercapacitor HESS which employs a filter-based power allocation method with an SCVC is presented [3], [22]. Then, it is shown that, due to the non-linearity of the SCVC, precise supercapacitor sizing and power allocation parameter selection is challenging. However, these issues can be overcome using an SCEC, which is described and analyzed later in the section.

A. HESS Operation With SCVC

The system configuration of the boost-inverter-based battery–supercapacitor HESS is shown in Fig. 1 [3], [22]. The objective of the converter is to generate a sinusoidal output voltage given by

$$v_o = V_o \sin(\omega t + \delta) \quad (1)$$

where V_o , ω and δ are the amplitude, frequency, and the phase angle of the inverter output voltage, respectively. The output capacitor voltages are controlled to follow the reference voltages $v_{o1,\text{ref}}$ and $v_{o2,\text{ref}}$ in order to generate the required differential output voltage v_o

$$v_{o1,\text{ref}} = V_{dc} + \frac{v_{o,\text{ref}}}{2} \quad v_{o2,\text{ref}} = V_{dc} - \frac{v_{o,\text{ref}}}{2} \quad (2)$$

where V_{dc} is the DC shift introduced to ensure $v_{o1,\text{ref}}$ and $v_{o2,\text{ref}}$ are always greater than the input voltages v_{batt} and v_{sc} . Subscripts 1 and 2 denote the left-hand-side and right-hand-side boost converter legs, respectively.

In this paper, two double-loop controllers are used to control the left-hand-side and right-hand-side boost converter legs as explained in [3], [37]. Each double-loop controller consists of an outer voltage control loop and two inner current control loops; one for the battery connected boost converter leg and another one for the supercapacitor connected boost converter leg.

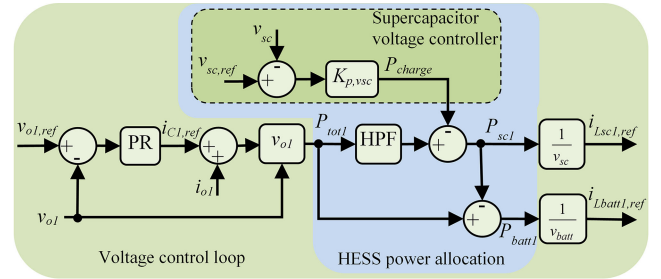


Fig. 2. Outer voltage control loop for the left-hand-side boost converter legs with SCVC.

The block diagram of the outer voltage control loop for the left-hand-side boost converter legs is shown in Fig. 2 [3]. A proportional resonant (PR) controller with a transfer function $H_{PR}(s)$ is employed to obtain better sinusoidal reference tracking performance [38]

$$H_{PR}(s) = K_{p,PR} + \frac{2sK_{i,PR}}{s^2 + \omega^2} \quad (3)$$

where $K_{p,PR}$ and $K_{i,PR}$ are the gains of the PR controller. In the voltage control loop, P_{tot1} is the total input power supplied by the left-hand-side boost converter legs. A high-pass filter is employed to allocate the high-frequency power variations to the supercapacitor. The high-pass filter transfer function is given by

$$H_{HPF}(s) = \frac{as}{as + 1} \quad (4)$$

where $1/a$ is the filter cut-off frequency in rad/s. The filtered power signal is then modified using the SCVC to maintain the supercapacitor voltage at around a reference voltage $v_{sc,\text{ref}}$ in order to avoid the supercapacitor overcharging or overdischarging.

The safe operating region of the supercapacitor is given by

$$v_{sc,min} \leq v_{sc} \leq v_{sc,max} \quad (5)$$

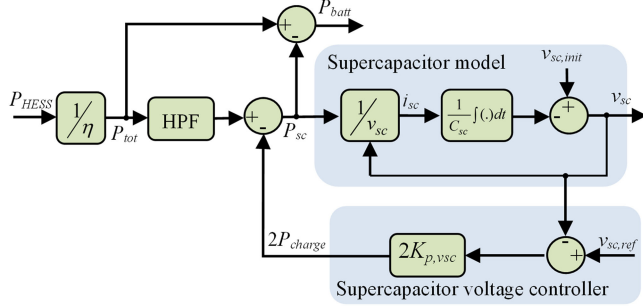


Fig. 3. Simplified block diagram of the HESS power allocation with the SCVC.

where $v_{sc,min}$ and $v_{sc,max}$ are the minimum and maximum allowed supercapacitor voltages, respectively.

The total power supplied by the left-hand-side and the right-hand-side boost converter legs is

$$P_{tot} = P_{tot1} + P_{tot2} = \frac{1}{\eta} P_{HES} \quad (6)$$

where P_{HES} is the total output power and η is the efficiency of the HESS.

In order to analyze the dynamic behavior of the HESS, a simplified model of the HESS power allocation method as illustrated in Fig. 3 is considered. In the simplified model, the supercapacitor is considered as an ideal capacitor by neglecting the equivalent series resistance (ESR) of the supercapacitor to simplify the analysis. The simplification can be made due to relatively small ESR of the supercapacitor. However, the simplification may have an impact on the analysis for high current applications with higher supercapacitor ESR [25], [39].

Using the simplified supercapacitor model, the relationship between the total power supplied by the supercapacitor P_{sc} and its voltage can be written as

$$v_{sc} = v_{sc,init} - \frac{1}{C_{sc}} \int \frac{P_{sc}}{v_{sc}} dt \quad (7)$$

where $v_{sc,init}$ and C_{sc} are the supercapacitor initial voltage and the capacitance of the supercapacitor, respectively. Since the SCVC modifies both the left-hand and right-hand-side boost converter leg power profiles, a factor of “2” is used in the SCVC model. Then, the relationship between P_{tot} and P_{sc} is given by

$$P_{sc} = HPF(P_{tot}) - 2K_{p,vsc} \left[(v_{sc,ref} - v_{sc,init}) + \int \frac{P_{sc}}{v_{sc} C_{sc}} dt \right] \quad (8)$$

where $HPF(P_{tot})$ is the output from the high-pass filter.

In order to design the high-pass filter and SCVC parameters and also to obtain the required energy storage elements sizes, the dynamic relationship between the P_{tot} and the power supplied by the individual energy storage devices (P_{sc} and P_{batt}) has to be obtained. However, due to nonlinearity in (7) and (8), it is challenging to obtain the relationship between P_{tot} and P_{sc} and also to size the supercapacitor C_{sc} . This problem can be overcome by replacing the SCVC with an SCEC as explained in the following sections.

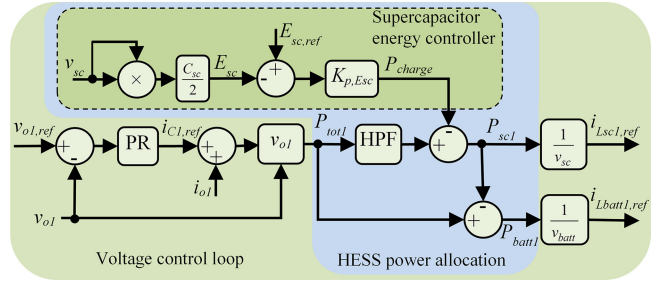


Fig. 4. Outer voltage control loop for the left-hand-side boost converter legs with SCEC.

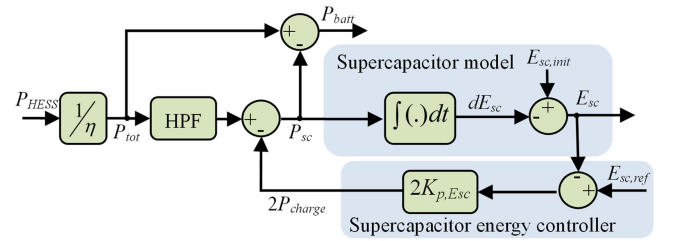


Fig. 5. Simplified block diagram of the HESS power allocation with the SCEC.

B. Supercapacitor Energy Controller

The modified outer voltage control loop for the left-hand-side boost converter legs with the SCEC is illustrated in Fig. 4. Instead of controlling the supercapacitor voltage v_{sc} , the energy stored in the supercapacitor E_{sc} is controlled around a reference energy level $E_{sc,ref}$. The stored energy in the supercapacitor E_{sc} is calculated as

$$E_{sc} = \frac{1}{2} C_{sc} v_{sc}^2. \quad (9)$$

In order to analyze the dynamic behavior of the power allocation method, a simplified model of the HESS power allocation with the SCEC, as shown in Fig. 5, is considered. Since the SCEC modifies both the left-hand and right-hand-side boost converter leg power profiles, a factor of “2” is used in the model. Using the simplified supercapacitor model, the relationship between the power supplied by the supercapacitor and its stored energy can be written as

$$E_{sc} = E_{sc,init} - \int P_{sc} dt \quad (10)$$

where $E_{sc,init}$ is the initial energy stored in the supercapacitor. Then using Fig. 5, power supplied by the supercapacitor can be obtained as

$$P_{sc}(s) = \frac{as^2}{as^2 + (1 + 2aK_{p,Esc})s + 2K_{p,Esc}} \frac{1}{\eta} P_{HES}(s) - \frac{2K_{p,Esc}s}{s + 2K_{p,Esc}} (E_{sc,ref}(s) - E_{sc,init}(s)). \quad (11)$$

Assuming

$$E_{sc,init} = E_{sc,ref} \quad (12)$$

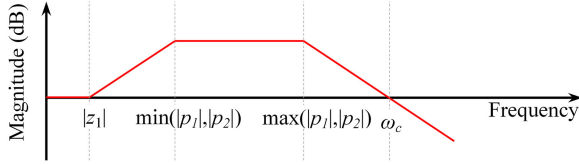


Fig. 6. Asymptotic Bode plot of the transfer function $H_{Pbatt}(s)$.

the transfer function between the $P_{HESS}(s)$ and $P_{sc}(s)$ can be found from (11) as

$$H_{Psc}(s) = \frac{P_{sc}(s)}{P_{HESS}(s)} = \frac{as^2}{as^2 + (1 + 2aK_{p,Esc})s + 2K_{p,Esc}\eta} \quad (13)$$

Similarly, the transfer function between the $P_{HESS}(s)$ and $P_{batt}(s)$ is

$$H_{Pbatt}(s) = \frac{P_{batt}(s)}{P_{HESS}(s)} = \frac{(1 + 2aK_{p,Esc})s + 2K_{p,Esc}}{as^2 + (1 + 2aK_{p,Esc})s + 2K_{p,Esc}\eta} \quad (14)$$

The transfer function between the supercapacitor energy change $dE_{sc}(s)$ and the HESS output power $P_{HESS}(s)$ can be found as

$$H_{dE_{sc}}(s) = \frac{dE_{sc}(s)}{P_{HESS}(s)} = \frac{as}{as^2 + (1 + 2aK_{p,Esc})s + 2K_{p,Esc}\eta} \quad (15)$$

C. Effect of the SCEC on the HESS Power Allocation Strategy

In this section, the derived transfer functions are further analyzed to identify the effects of the SCEC on the filter-based HESS power allocation strategy.

It can be observed that (14) has a zero z_1 and two poles p_1 and p_2

$$z_1 = \frac{-2K_{p,Esc}}{1 + 2aK_{p,Esc}} \quad p_1 = -\frac{1}{a} \quad p_2 = -2K_{p,Esc}. \quad (16)$$

It can be shown that

$$|z_1| < |p_1| \text{ and } |z_1| < |p_2| \quad (17)$$

for positive, nonzero a and $K_{p,Esc}$ values. Using the aforementioned relationships, an asymptotic Bode plot of $H_{Pbatt}(s)$ can be drawn as in Fig. 6. Then, the following relationship can be found:

$$\frac{\omega_c}{\max(|p_1|, |p_2|)} = \frac{\min(|p_1|, |p_2|)}{(|z_1|)} \quad (18)$$

where ω_c is the gain cross-over frequency of $H_{Pbatt}(s)$.

Using (16) and (18)

$$\omega_c = \frac{1 + 2aK_{p,Esc}}{a}. \quad (19)$$

By substituting $K_{p,Esc} = 0$ to (19), the gain cross-over frequency corresponding to the HESS operation without any supercapacitor SoC control method is

$$\omega'_c = \frac{1}{a} \quad (20)$$

which is similar to the high-pass filter cut-off frequency. Super-script ' denotes the HESS operation without any supercapacitor

SoC control method. By comparing (19) and (20), it can be observed that due to the introduction of SCEC, the gain cross-over frequency is modified by a factor of $(1 + 2aK_{p,Esc})$ and hence it is evident that the SCEC has a significant effect on the HESS power allocation. To further investigate the effect, (14) can be rewritten as

$$H_{Pbatt}(s) = \left[\frac{\omega_c s + \gamma}{s^2 + \omega_c s + \gamma} \right] \frac{1}{\eta} \quad (21)$$

where

$$\gamma = \frac{2K_{p,Esc}}{a}. \quad (22)$$

Assume that the required $H_{Pbatt}(s)$ gain cross-over frequency is $\omega_{c,req}$. Then, the HESS power allocation parameters a and $K_{p,Esc}$ have to be selected such that

$$\frac{1 + 2aK_{p,Esc}}{a} = \omega_{c,req}. \quad (23)$$

However, it can be observed from (21) that infinite number of $H_{Pbatt}(s)$ transfer functions with $\omega_{c,req}$ gain cross-over frequency can be obtained by changing the γ value. Substituting $K_{p,Esc}$ from (22) into (23) and solving for a gives

$$a = \frac{\omega_{c,req} \pm \sqrt{\omega_{c,req}^2 - 4\gamma}}{2\gamma}. \quad (24)$$

From (24), it can be observed that there are two combinations of a and $K_{p,Esc}$ values that lead to the same $H_{Pbatt}(s)$ transfer function. Further from (24), for a required gain cross-over frequency $\omega_{c,req}$, γ has to satisfy

$$0 \leq \gamma \leq \frac{\omega_{c,req}^2}{4}. \quad (25)$$

Using

$$n = \frac{\gamma}{\omega_{c,req}^2} \quad (26)$$

and (25), all possible $H_{Pbatt}(s)$ transfer functions with $\omega_{c,req}$ gain cross-over frequency can be obtained by changing n in the range of

$$0 \leq n \leq 0.25. \quad (27)$$

Subsequently, the effect of n on the HESS dynamic performance is studied. Fig. 7(a) and (b) illustrates the effect of n on the step response of $H_{Pbatt}(s)$ and $H_{dE_{sc}}(s)$ for a sample gain cross-over frequency $\omega_{c,req} = 0.05$ rad/s. When $n = 0$, the supercapacitor energy is not controlled and as expected it does not reach the reference value (at the steady state $dE_{sc} \neq 0$). The fastest battery response and the minimum supercapacitor energy change occurs for $n = 0.25$.

D. Calculating the Capacitance of the Supercapacitor for a Set of HESS Power Allocation Parameters

Next, the supercapacitor value calculation for a set of HESS power allocation parameters ($\omega_{c,req}$ and n) for a given HESS power profile is presented. First, the maximum and minimum supercapacitor voltage limits $v_{sc,max}$ and $v_{sc,min}$ have to be

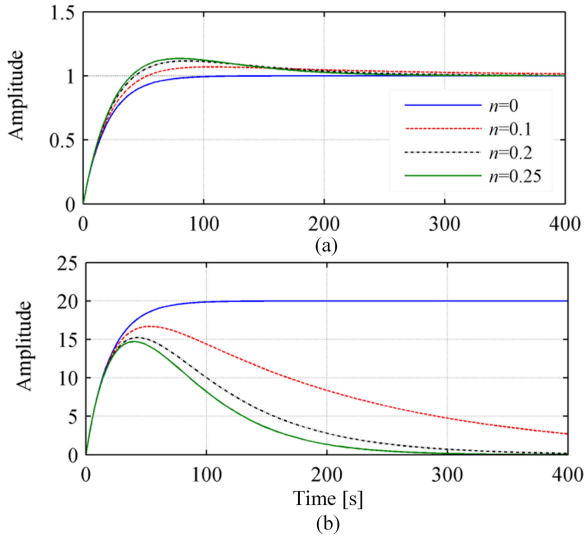


Fig. 7. Step response of (a) $H_{Pbatt}(s)$ and (b) $H_{dE_{sc}}(s)$ for various n values for a sample gain cross-over frequency $\omega_{c,req} = 0.05$ rad/s.

determined based on the power converter specifications. In the considered boost-inverter-based HESS, $v_{sc,min}$ is determined by the maximum possible gain of the converter while $v_{sc,max}$ has to satisfy

$$v_{sc,max} \leq V_{dc} - \frac{V_o}{2}. \quad (28)$$

Using the maximum and minimum supercapacitor voltage limits $v_{sc,max}$ and $v_{sc,min}$, the utilized energy of the supercapacitor $E_{sc,u}$ can be calculated as

$$E_{sc,u} = E_{sc,max} - E_{sc,min} = 0.5C_{sc}(v_{sc,max}^2 - v_{sc,min}^2) \quad (29)$$

where $E_{sc,max}$ and $E_{sc,min}$ are the supercapacitor energy levels corresponding to the voltage limits $v_{sc,max}$ and $v_{sc,min}$, respectively.

If the supercapacitor reference energy level is selected as

$$E_{sc,ref} = E_{sc,min} + 0.5E_{sc,u} \quad (30)$$

then equal amount of energy ($0.5 E_{sc,u}$) is available for both the supercapacitor charging and discharging. The supercapacitor voltage corresponding to $E_{sc,ref}$ is given by

$$v_{sc,ref} = \sqrt{0.5(v_{sc,min}^2 + v_{sc,max}^2)}. \quad (31)$$

Then, using the considered HESS power profile and the set of HESS power allocation parameters ($\omega_{c,req}$ and n), the supercapacitor energy variation profile dE_{sc} can be obtained using the transfer function (15). Since only half of the utilized energy is available for either the supercapacitor charging or discharging

$$0.5E_{sc,u} = \max(|dE_{sc}|). \quad (32)$$

Then, the required supercapacitor value for the considered power profile and for the set of power allocation parameters can be obtained as

$$C_{sc} = \frac{4\max(|dE_{sc}|)}{v_{sc,max}^2 - v_{sc,min}^2}. \quad (33)$$

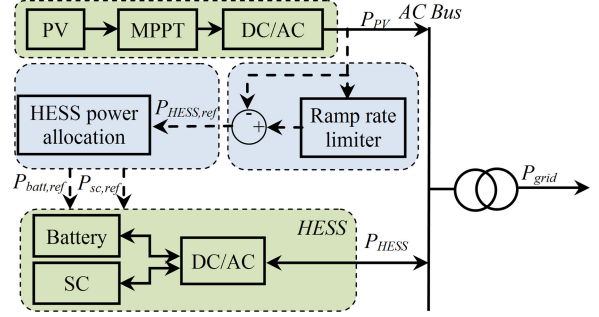


Fig. 8. Block diagram of the HESS in a PV power smoothing application.

However, it has to be noted that in high current applications with higher supercapacitor ESR the SCEC will not comply with the voltage limits $v_{sc,max}$ and $v_{sc,min}$ due to the voltage drop across the ESR [25], [39].

III. HESS POWER ALLOCATION PARAMETER SELECTION AND SUPERCAPACITOR SIZING FOR A PV POWER SMOOTHING APPLICATION

In this section, a case study to illustrate the HESS power allocation parameter calculation and supercapacitor sizing for a filter-based HESS with the SCEC in a PV power smoothing application is presented. The power allocation parameters are calculated to minimize the required supercapacitor value while achieving the required smoothness of the battery power profile. Later in the section, the required supercapacitor values for the HESS operation with the SCVC are estimated and compared against the HESS operation with the SCEC.

As mentioned in Section I, the lifetime of a battery can be extended by smoothing the battery power profile. In this paper, the smoothness of the battery power profile is achieved by limiting the variability in the battery power profile. As a measure of variability, the gradient of the battery power profile is considered.

Fig. 8 illustrates an example application when the HESS is used to smooth the power delivered to the grid at the common coupling point. The PV power profile is selected from data available in [40] and scaled to match the experimental setup parameters given in Section V. The HESS power profile is obtained as the difference between the generated PV power and the power supplied to the grid. Since the PV power smoothing is not the main focus of this paper, a simple rate limiter is used to limit the per minute ramp rate to 10% of the rated power of the PV plant [41]. Relevant power profiles are illustrated in Fig. 9. In Fig. 9(a), P_{PV} , P_{grid} , and P_{HESS} are the generated power profile from the PV plant, power injected to the grid, and the compensating power supplied by the HESS, respectively. Fig. 9(b) illustrates the total power supplied by the battery and the supercapacitor P_{tot} . In order to quantify the variability of the P_{tot} power profile, the gradient of the power profile $|\nabla P_{tot}|$

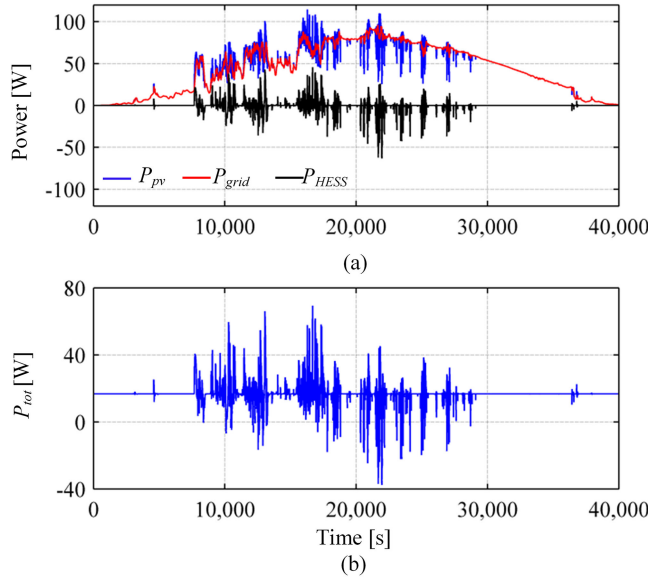


Fig. 9. Power profiles considered for the HESS parameter selection. (a) PV power, power injected to the grid and the HESS power and (b) the total power profile of the battery and the supercapacitor.

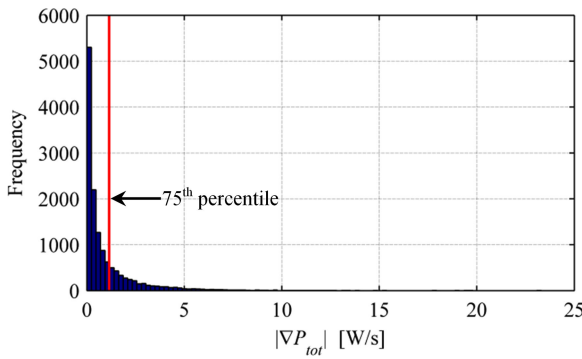


Fig. 10. Histogram of the nonzero gradient values of the \$P_{tot}\$ power profile

is considered. The histogram of nonzero gradient values of the \$P_{tot}\$ power profile \$|\nabla P_{tot}|\$ is shown in Fig. 10.

By selecting the HESS power allocation parameters \$\omega_c\$ and \$n\$, the higher gradient power variations in \$P_{tot}\$ power profile can be allocated to the supercapacitor. For that, the relationship between the HESS power allocation parameters and the battery power profile gradient has to be identified first.

To observe the relationship between the battery power gradient and the HESS power allocation parameters \$\omega_c\$ and \$n\$, a set of battery power profiles is obtained using the \$P_{HESS}\$ power profile in Fig. 9 and (21) for a set of \$\omega_c\$ and \$n\$ values. Then, the maximum gradient of the battery power profile \$\max(|\nabla P_{batt}|)\$ is plotted against \$\omega_c\$ and \$n\$ as shown in Fig. 11(a). Additionally, the required supercapacitor values for each set of \$\omega_c\$ and \$n\$ are calculated and illustrated in Fig. 11(b).

Then, a linear search method using the data in Fig. 11(a) and (b) is employed to obtain the required HESS power allocation parameters (\$\omega_{c,req}\$ and \$n_{req}\$), which minimize the required supercapacitor value \$C_{sc}\$, subject to \$\max(|\nabla P_{batt}|) \leq

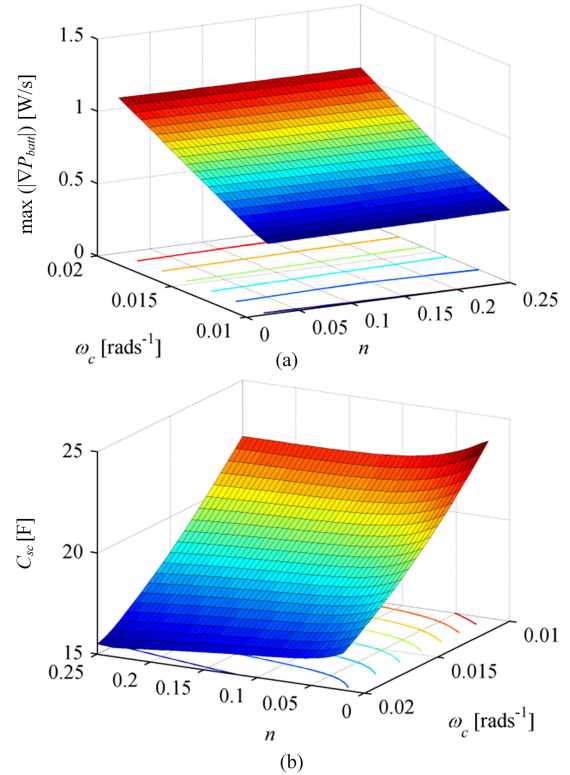


Fig. 11. Variation of (a) \$\max(|\nabla P_{batt}|)\$ and (b) \$C_{sc}\$ with \$n\$ and \$\omega_c\$.

\$\nabla P_{batt,limit}\$. Here, \$\nabla P_{batt,limit}\$ is a predefined maximum allowable gradient for the battery power profile. In the linear search method, first a set of \$\omega_c\$ and \$n\$ values, which satisfy the condition \$\max(|\nabla P_{batt}|) \leq \nabla P_{batt,limit}\$, is selected and then the power allocation parameters corresponding to the minimum required supercapacitor value \$C_{sc,req}\$ in the selected set are identified. Once the required \$\omega_{c,req}\$ and \$n_{req}\$ are found, the high-pass filter parameter \$a\$ and the SCEC gain \$K_{p,Esc}\$ can be found using (18), (23), and (25) as

$$a = \frac{\omega_{c,req} + \sqrt{\omega_{c,req}^2 - 4n_{req}\omega_{c,req}^2}}{2n_{req}\omega_{c,req}^2} \quad (34)$$

$$K_{p,Esc} = \frac{a\omega_{c,req} - 1}{2a}. \quad (35)$$

Table I summarizes the HESS power allocation parameters \$a\$ and \$K_{p,Esc}\$ and the required supercapacitor values \$C_{sc,req}\$ obtained for various \$\nabla P_{batt,limit}\$ values. The \$\nabla P_{batt,limit}\$ is calculated as the \$\rho^{th}\$ percentile value of the nonzero gradient values of the \$P_{tot}\$ power profile. The considered supercapacitor voltage limits \$v_{sc,min}\$ and \$v_{sc,max}\$ are given in Table II.

Fig. 12 illustrates the operation of the HESS with the values selected for the 75th percentile value. Fig. 12(a) demonstrates that the battery supplies only the low-frequency power component of \$P_{tot}\$ power variation. The selected HESS parameters ensure the battery power gradient remains within the \$\pm \nabla P_{batt,limit}\$ values as shown in Fig. 12(b). SCEC maintains the supercapacitor energy variation around the reference energy

TABLE I
HESS POWER ALLOCATION PARAMETERS AND SUPERCAPACITOR VALUES FOR VARIOUS $\nabla P_{batt,limit}$ VALUES WITH AND WITHOUT SCEC

ρ	$\nabla P_{batt,limit}$ (W/s)	HESS Operation with SCEC			HESS Operation Without Supercapacitor SoC Controller	
		a	$K_{p,Esc}$	$C_{sc,req}$ [F]	a'	$C'_{sc,req}$ [F]
90 th	2.5863	244.88	0.0230	8.35	19.42	11.09
85 th	1.9098	325.82	0.0160	11.13	28.57	15.28
80 th	1.4571	191.89	0.0099	13.66	37.74	18.83
75 th	1.1451	132.44	0.0062	15.44	47.62	22.06
70 th	0.8979	117.65	0.0043	16.97	60.61	25.60
65 th	0.7177	142.86	0.0035	18.96	71.43	28.25
60 th	0.5825	628.57	0.0052	20.77	86.96	31.79

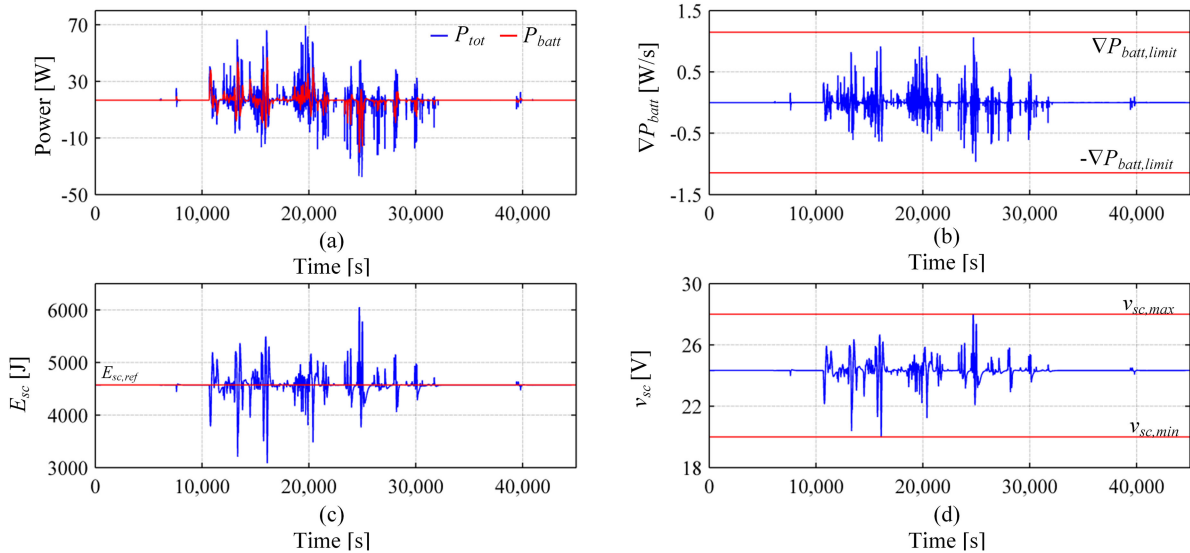


Fig. 12. Operation of the HESS when $\rho = 75$. (a) P_{tot} and P_{batt} power profiles, (b) gradient of the battery power profile, (c) supercapacitor energy variation, and (d) voltage variation of the supercapacitor.

TABLE II
HESS PROTOTYPE PARAMETERS

Parameter	Value	Parameter	Value
<i>Power converter parameters</i>			
V_o	60 V	V_{dc}	60 V
L_{batt1}, L_{batt2}	$210 \mu\text{H}$	L_{sc1}, L_{sc2}	$210 \mu\text{H}$
C_1, C_2	$60 \mu\text{F}$	f	50 Hz
$v_{sc,max}$	28 V	$v_{sc,min}$	20 V
<i>Grid parameters</i>			
V_g	60 V	L_g	20 mH
<i>Voltage control loop parameters</i>			
$K_{p,PR}$	0.1	$K_{i,PR}$	4
<i>Current control loop parameters</i>			
$K_{p,PI2,batt}$	2.615	$K_{p,PI2,sc}$	2.615
$K_{i,PI2,batt}$	8.44×10^{-5}	$K_{p,PI2,sc}$	8.44×10^{-5}
<i>PQ controller parameters</i>			
$K_{p,PI,P}$	2×10^{-6}	$K_{i,PI,P}$	0.14
$K_{p,PI,Q}$	1×10^{-5}	$K_{i,PI,Q}$	4

level as shown in Fig. 12(c) and as required the HESS operates without violating the supercapacitor voltage limits, as shown in Fig. 12(d).

Next, the supercapacitor sizing and HESS power allocation parameter selection corresponding to the HESS operation with the SCVC is considered. As mentioned in Section II, when the conventional SCVC is used, it is difficult to size the supercapacitor. Hence, the only way to estimate a suitable size of the supercapacitor is to size it without considering the supercapacitor SoC controller. The transfer function between the supercapacitor energy change $dE'_{sc}(s)$ and $P_{HESS}(s)$ for the operation of the HESS without the supercapacitor SoC controller is given by

$$H'_{dE_{sc}}(s) = \frac{dE'_{sc}(s)}{P_{HESS}(s)} = \left(\frac{a'}{a's + 1} \right) \frac{1}{\eta} = \left(\frac{1/\omega'_c}{1/\omega'_c s + 1} \right) \frac{1}{\eta}. \quad (36)$$

The superscript ' denotes the HESS operation without the supercapacitor SoC controller. The power allocation frequency ω'_c is similar to the high-pass filter cut-off frequency $1/a'$. The supercapacitor energy variation dE'_{sc} for the considered output power profile and for any ω'_c value can be obtained using (36). Then, the relevant supercapacitor value can be calculated as

$$C'_{sc} = \frac{4\max(|dE'_{sc}|)}{v_{sc,max}^2 - v_{sc,min}^2}. \quad (37)$$

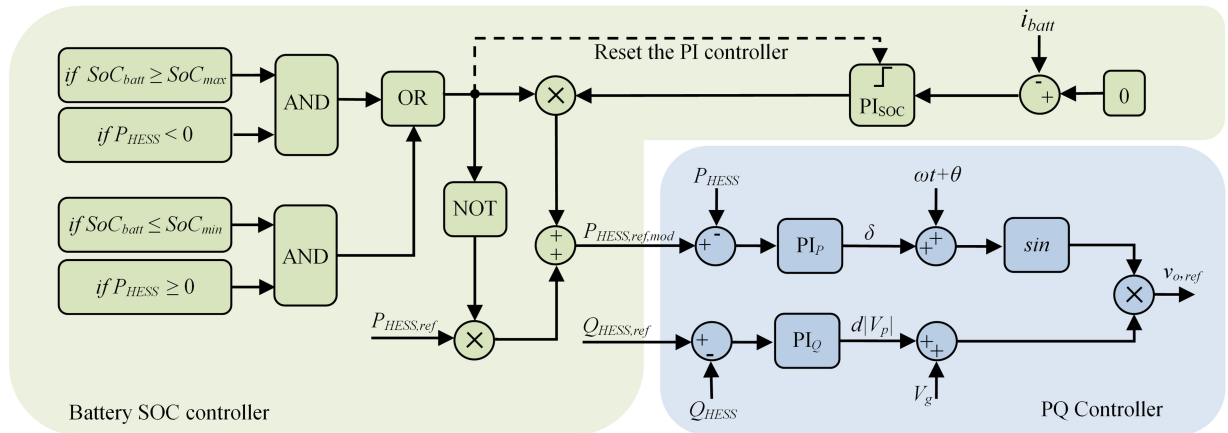


Fig. 13. HESS active/reactive power controller with battery SoC management system.

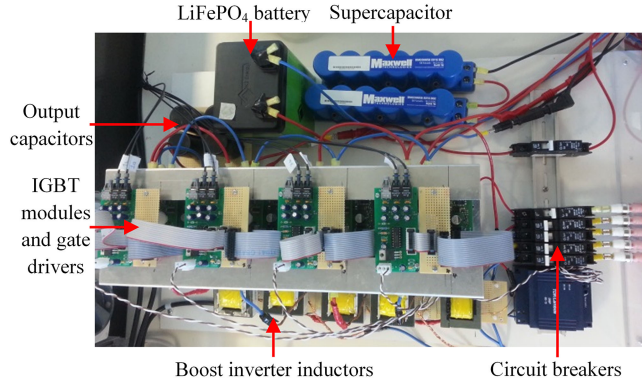


Fig. 14. HESS experimental setup.

Similar to the operation of the HESS with the SCEC, the required power allocation frequency $\omega_{c,req}$ is obtained to minimize the supercapacitor value C'_{sc} , subject to $\max(|\nabla P'_{batt}|) \leq \nabla P_{batt,limit}$. The corresponding minimum required supercapacitor values $C'_{sc,req}$ are compared in Table I, with $C_{sc,req}$ values calculated for the HESS operation with the SCEC. Clearly, using the SCEC not only allows precise sizing of the supercapacitor but also the required capacitance of the supercapacitor is significantly lower than the one estimated for the SCVC.

IV. HESS CONTROL SYSTEM AND EXPERIMENTAL RESULTS

In this paper, two double-loop controllers are used to control the left-hand-side and right-hand-side boost converter legs as explained in [3]. Active and reactive power supplied by the HESS is controlled by modifying the inverter output voltage amplitude and the phase angle with respect to the grid voltage, as shown in Fig. 13 [3]. The double-loop controller parameters and the active/reactive power controller parameters are summarized in Table II.

In order to validate the effects of the SCEC on the filter-based HESS, the experimental prototype shown in Fig. 14 was used. A 9.6 Ah, 25.6 V LiFePO₄ battery was used in the prototype.

The controllers were implemented on a DSpace DS1006 platform using MATLAB/Simulink. The HESS was connected to a single-phase AC grid using a step-up transformer. Parameters of the HESS and controllers are summarized in Table II.

A 900 s HESS power profile in Fig. 15(a) was considered in the experiment. For the HESS parameter calculation, $\nabla P_{batt,limit}$ was chosen as the 75th percentile of the nonzero gradient values of the P_{tot} power profile (0.6986 W/s). Then, using the linear search method explained in Section IV, the required HESS power allocation parameters were obtained as $\omega_{c,req} = 0.013$ rad/s and $n_{req} = 0.208$. The required a and $K_{p,Esc}$ values were calculated as 255.81 and 0.0045, respectively. For the obtained HESS power allocation parameters, the required supercapacitor value is 27.19 F. Hence, a commercially available 29 F supercapacitor (two series connected 58 F Maxwell supercapacitor modules) was used in the experiments.

Fig. 15 illustrates the operation of the HESS with the obtained power allocation parameters and the 29F supercapacitor. According to Fig. 15(b) the battery supplies the slow varying power component of the P_{tot} while the supercapacitor supplies the rapid power changes. The maximum gradient of the P_{tot} power profile ∇P_{tot} in Fig. 15(c) is close to 20W/s which is clearly above the $\nabla P_{batt,limit}$ value. However, as required, the battery power gradient remains within the $\pm \nabla P_{batt,limit}$ limits, as illustrated in Fig. 15(d). The energy variation of the supercapacitor is shown in Fig. 15(e). The energy is controlled around the reference energy level $E_{sc,ref}$ by the SCEC, limiting the risk of the supercapacitor overcharging or overdischarging. Fig. 15(f) depicts the variation of the supercapacitor voltage, which lies within the specified maximum and minimum supercapacitor voltage limits throughout the experiment. The battery and supercapacitor current profiles are shown in Fig. 15(g) and (h). As expected, the battery supplies the slow varying current while the supercapacitor supplies the high-frequency current requirement. Moreover, it can be observed from Fig. 15(b) and (g) that by limiting the gradient of the battery power profile, the peak battery power and the number of charge/discharge cycles of the battery are reduced.

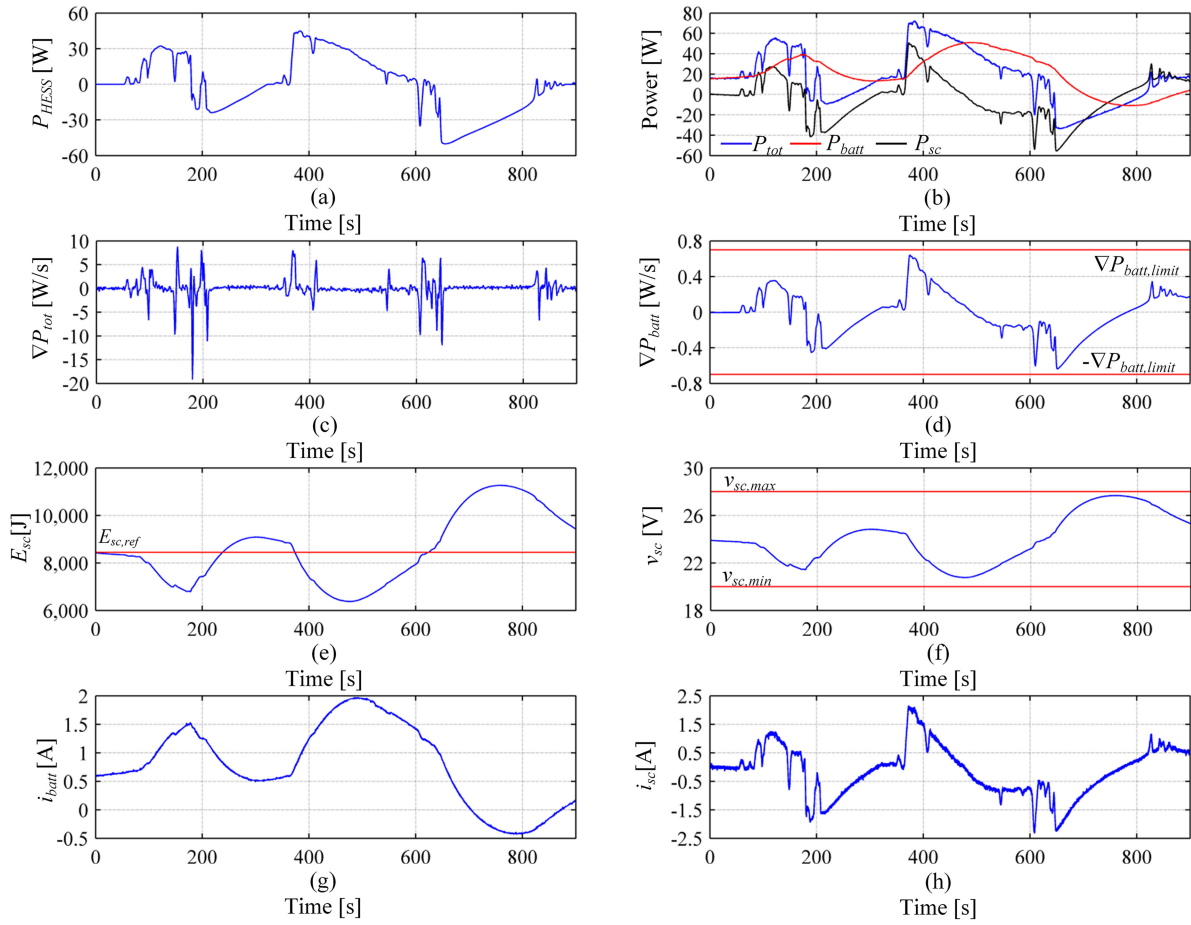


Fig. 15. Operation of the HESS with SCEC (a) power reference of the HESS, (b) variation of P_{tot} , P_{batt} , and P_{sc} , (c) gradient of the P_{tot} profile, (d) gradient of the battery power profile, (e) supercapacitor energy variation, (f) supercapacitor voltage variation, (g) battery current variation, and (h) supercapacitor current variation.

V. CONCLUSION

The main disadvantage of using the SCVC in filter-based HESSs is difficulty in selecting the filter parameters and sizing the supercapacitor. In this paper, it was proposed to use the SCEC to control the supercapacitor energy instead of its voltage. This facilitated to develop a method, which allows precise selection of the filter parameters and sizing of the supercapacitor for a given application. Additional benefit is that the size of the supercapacitor is significantly lower than the one estimated when the SCVC is used. Application of the proposed method was illustrated and experimentally verified for a PV power smoothing application using a single-phase grid-connected HESS. Presented results showed that the HESS operated within the required power variation and supercapacitor voltage limits.

REFERENCES

- [1] J. Cao and A. Emadi, "A new battery/ultracapacitor hybrid energy storage system for electric, hybrid, and plug-in hybrid electric vehicles," *IEEE Trans. Power Electron.*, vol. 27, no. 1, pp. 122–132, Jan. 2012.
- [2] B. Hredzak, V. G. Agelidis, and G. D. Demetriades, "A low complexity control system for a hybrid DC power source based on ultracapacitor-lead acid battery configuration," *IEEE Trans. Power Electron.*, vol. 29, no. 6, pp. 2882–2891, Jun. 2014.
- [3] D. B. W. Abeywardana, B. Hredzak, and V. G. Agelidis, "Single-phase grid-connected LiFePO₄ battery-supercapacitor hybrid energy storage system with interleaved boost inverter," *IEEE Trans. Power Electron.*, vol. 30, no. 10, pp. 5591–5604, Oct. 2015.
- [4] N. Mendis, K. M. Muttaqi, and S. Perera, "Management of low- and high-frequency power components in demand-generation fluctuations of a DFIG-based wind-dominated RAPS system using hybrid energy storage," *IEEE Trans. Ind. Appl.*, vol. 50, no. 3, pp. 2258–2268, May/Jun. 2014.
- [5] S. S. G. Jayasinghe, D. M. Vilathgamuwa, and U. K. Madawala, "Diode-clamped three-level inverter-based battery/supercapacitor direct integration scheme for renewable energy systems," *IEEE Trans. Power Electron.*, vol. 26, no. 12, pp. 3720–3729, Dec. 2011.
- [6] B. Hredzak, V. G. Agelidis, and J. Minsoo, "A model predictive control system for a hybrid battery-ultracapacitor power source," *IEEE Trans. Power Electron.*, vol. 29, no. 3, pp. 1469–1479, Mar. 2014.
- [7] O. Laldin, M. Moshirvaziri, and O. Trescases, "Predictive algorithm for optimizing power flow in hybrid ultracapacitor/battery storage systems for light electric vehicles," *IEEE Trans. Power Electron.*, vol. 28, no. 8, pp. 3882–3895, Aug. 2013.
- [8] L. Baoquan, Z. Fang, and B. Xianwen, "Fuzzy control for hybrid energy storage system based on battery and ultra-capacitor in micro-grid," in *Proc. 2012 7th Int. Power Electron. Motion Control Conf.*, 2012, pp. 778–782.
- [9] M. Zandi, A. Payman, J. P. Martin, S. Pierfederici, B. Davat, and F. Meibody-Tabar, "Energy management of a fuel cell/supercapacitor/battery power source for electric vehicular applications," *IEEE Trans. Veh. Technol.*, vol. 60, no. 2, pp. 433–443, Feb. 2011.
- [10] C. Abbey, K. Strunz, and G. Joos, "A knowledge-based approach for control of two-level energy storage for wind energy systems," *IEEE Trans. Energy Convers.*, vol. 24, no. 2, pp. 539–547, Jun. 2009.

- [11] J. Moreno, M. E. Ortuzar, and J. W. Dixon, "Energy-management system for a hybrid electric vehicle, using ultracapacitors and neural networks," *IEEE Trans. Ind. Electron.*, vol. 53, no. 2, pp. 614–623, Apr. 2006.
- [12] A. Kuperman, I. Aharon, S. Malki, and A. Kara, "Design of a semi-active battery-ultracapacitor hybrid energy source," *IEEE Trans. Power Electron.*, vol. 28, no. 2, pp. 806–815, Feb. 2013.
- [13] M. A. Tankari, M. B. Camara, B. Dakyo, and G. Lefebvre, "Use of ultracapacitors and batteries for efficient energy management in wind diesel hybrid system," *IEEE Trans. Sustain. Energy*, vol. 4, no. 2, pp. 414–424, Apr. 2013.
- [14] Y. Zhang, X. Tang, Z. Qi, and Z. Liu, "The ragone plots guided sizing of hybrid storage system for taming the wind power," *Int. J. Elect. Power Energy Syst.*, vol. 65, pp. 246–253, 2015.
- [15] A. Lahyani, P. Venet, A. Guermazi, and A. Troudi, "Battery-supercapacitors combination in uninterruptible power supply (UPS)," *IEEE Trans. Power Electron.*, vol. 28, no. 4, pp. 1509–1522, Apr. 2013.
- [16] R. Esteves Araujo, R. De Castro, C. Pinto, P. Melo, and D. Freitas, "Combined sizing and energy management in EVs with batteries and supercapacitors," *IEEE Trans. Veh. Technol.*, vol. 63, no. 7, pp. 3062–3076, Sep. 2014.
- [17] Q. Jiang and H. Hong, "Wavelet-based capacity configuration and coordinated control of hybrid energy storage system for smoothing out wind power fluctuations," *IEEE Trans. Power Syst.*, vol. 28, no. 2, pp. 1363–1372, May 2013.
- [18] J. Shen, S. Dusmez, and A. Khaligh, "Optimization of sizing and battery cycle life in battery/ultracapacitor hybrid energy storage systems for electric vehicle applications," *IEEE Trans. Ind. Informat.*, vol. 10, no. 4, pp. 2112–2121, Nov. 2014.
- [19] F. Ongaro, S. Saggini, and P. Mattavelli, "Li-ion battery-supercapacitor hybrid storage system for a long lifetime, photovoltaic-based wireless sensor network," *IEEE Trans. Power Electron.*, vol. 27, no. 9, pp. 3944–3952, Sep. 2012.
- [20] E. Schaltz, A. Khaligh, and P. O. Rasmussen, "Influence of battery/ultracapacitor energy-storage sizing on battery lifetime in a fuel cell hybrid electric vehicle," *IEEE Trans. Veh. Technol.*, vol. 58, no. 8, pp. 3882–3891, Oct. 2009.
- [21] J. Bauman and M. Kazerani, "A comparative study of fuel-cell-battery, fuel-cell-ultracapacitor, and fuel-cell-battery-ultracapacitor vehicles," *IEEE Trans. Veh. Technol.*, vol. 57, no. 2, pp. 760–769, Mar. 2008.
- [22] D. B. W. Abeywardana, B. Hredzak, and V. G. Agelidis, "A single phase grid integration scheme for battery-supercapacitor AC line hybrid storage system," presented at the *IEEE Int. Conf. Ind. Technol.*, Busan, 2014, pp. 235–240.
- [23] A. Kuperman and I. Aharon, "Battery-ultracapacitor hybrids for pulsed current loads: A review," *Renewable Sustain. Energy Rev.*, vol. 15, pp. 981–992, 2011.
- [24] A. Kuperman, I. Aharon, A. Kara, and S. Malki, "A frequency domain approach to analyzing passive battery-ultracapacitor hybrids supplying periodic pulsed current loads," *Energy Convers. Manag.*, vol. 52, pp. 3433–3438, 2011.
- [25] V. Yuhimenko, C. Lerman, and A. Kuperman, "DC active power filter based hybrid energy source for pulsed power loads," *IEEE J. Emerging Sel. Topics Power Electron.*, vol. 3, no. 4, pp. 1001–1010, Dec. 2015.
- [26] S. Fiorenti, J. Guanetti, Y. Guezennec, and S. Onori, "Modeling and experimental validation of a hybridized energy storage system for automotive applications," *J. Power Sources*, vol. 241, pp. 112–120, Jan. 11, 2013.
- [27] S. Fiorenti, Y. Guezennec, S. Onori, N. Madella, A. Saletti, and S. Bovo, "Modeling and experimental validation of PbA battery-supercapacitor energy storage system," presented at the 7th IFAC Symp. Advances Autom. Control, Tokyo, Japan, 2013.
- [28] I. Aharon and A. Kuperman, "Topological overview of powertrains for battery-powered vehicles with range extenders," *IEEE Trans. Power Electron.*, vol. 26, no. 3, pp. 868–876, Mar. 2011.
- [29] K. W. Wee, S. S. Choi, and D. M. Vilathgamuwa, "Design of a least-cost battery-supercapacitor energy storage system for realizing dispatchable wind power," *IEEE Trans. Sustain. Energy*, vol. 4, no. 3, pp. 786–796, Jul. 2013.
- [30] A. M. Gee, F. V. P. Robinson, and R. W. Dunn, "Analysis of battery lifetime extension in a small-scale wind-energy system using supercapacitors," *IEEE Trans. Energy Convers.*, vol. 28, no. 1, pp. 24–33, Mar. 2013.
- [31] E. M. Krieger, J. Cannarella, and C. B. Arnold, "A comparison of lead-acid and lithium-based battery behavior and capacity fade in off-grid renewable charging applications," *Energy*, vol. 60, no. 1, pp. 492–500, Oct. 2013.
- [32] L. Goemaere, A. Soares, C. M. Ionica-Bousquet, Y. Thiaux, L. Stievano, C. Glaize *et al.*, "Studying the electrochemical response to emulated photovoltaic electrochemical constraints of Li-ion electrode materials at the lab-scale," *J. Power Sources*, vol. 196, no. 20, pp. 8688–8691, Oct. 2011.
- [33] M. Dubarry and B. Y. Liaw, "Identify capacity fading mechanism in a commercial LiFePO₄ cell," *J. Power Sources*, vol. 194, pp. 541–549, Oct. 2009.
- [34] C. Masjosthusmann, N. Decius, X. Köhler, and U. Büker, "Smoothing the battery current in battery electric vehicles using a quantitative feedback theory designed MIMO-controller," in *Proc. IET Hybrid Elect. Vehicles Conf.*, 2013, pp. 1–6.
- [35] F. Ciccarelli, A. Del Pizzo, and D. Iannuzzi, "Improvement of energy efficiency in light railway vehicles based on power management control of wayside lithium-ion capacitor storage," *IEEE Trans. Power Electron.*, vol. 29, pp. 275–286, 2014.
- [36] J. Pegueroles-Queralt, F. D. Bianchi, and O. Gomis-Bellmunt, "A power smoothing system based on supercapacitors for renewable distributed generation," *IEEE Trans. Ind. Electron.*, vol. 62, pp. 343–350, 2015.
- [37] P. Sanchis, A. Ursaea, E. Gubia, and L. Marroyo, "Boost DC-AC inverter: A new control strategy," *IEEE Trans. Power Electron.*, vol. 20, pp. 343–353, 2005.
- [38] R. Teodorescu, F. Blaabjerg, M. Liserre, and P. C. Loh, "Proportional-resonant controllers and filters for grid-connected voltage-source converters," in *Proc. IEE Elect. Power Appl.*, 2006, vol. 153, pp. 750–762.
- [39] A. Kuperman, M. Mellincovsky, C. Lerman, I. Aharon, N. Reichbach, G. Geula *et al.*, "Supercapacitor sizing based on desired power and energy performance," *IEEE Trans. Power Electron.*, vol. 29, pp. 5399–5405, 2014.
- [40] NREL. National Renewable Energy Laboratory-Measurement and Instrumentation Data Center. (2011). [Online]. Available: http://www.nrel.gov/midc/oahu_archive/
- [41] J. Marcos, O. Storkel, L. Marroyo, M. Garcia, and E. Lorenzo, "Storage requirements for PV power ramp-rate control," *Solar Energy*, vol. 99, pp. 28–35, 2014.



Damith Buddika Wickramasinghe Abeywardana (S'12) received the B.Sc. degree in electrical and electronic engineering from the University of Peradeniya, Peradeniya, Sri Lanka. He is currently working towards the Ph.D. degree in electrical engineering at the University of New South Wales, Sydney, Australia.

His current research interests include hybrid energy storage systems, renewable energy integration, and smart grids. His research work is also engaged with the Australian Energy Research Institute (AERI), Sydney, Australia.



Branislav Hredzak (M'98–SM'13) received the B.Sc./M.Sc. degree from the Technical University of Kosice, Kosice, Slovak Republic, in 1993, and the Ph.D. degree from Napier University of Edinburgh, Edinburgh, U.K., in 1997, all in electrical engineering.

He was as a Lecturer and a Senior Researcher in Singapore from 1997 to 2007. He is currently a Senior Lecturer in the School of Electrical Engineering and Telecommunications, The University of New South Wales, Sydney, Australia. His current research interests include hybrid storage technologies and advanced control systems for power electronics and storage systems.



Vassilios G. Agelidis (SM'00) was born in Serres, Greece. He received the B.Eng. degree in electrical engineering from the Democritus University of Thrace, Thrace, Greece, in 1988, the M.S. degree in applied science from Concordia University, Montreal, QC, Canada, in 1992, and the Ph.D. degree in electrical engineering from Curtin University, Perth, WA, Australia, in 1997. He was with Curtin University (1993–1999), the University of Glasgow, U.K. (2000–2004), Murdoch University, Perth (2005–2006), and the University of Sydney, Australia (2007–2010). He is currently the Director of the Australian Energy Research Institute, University of New South Wales (UNSW), Sydney, Australia.

Dr. Agelidis received the Advanced Research Fellowship from the U.K.'s Engineering and Physical Sciences Research Council in 2004. He was the Vice-President Operations within the IEEE Power Electronics Society from 2006 to 2007. He was an AdCom Member of IEEE PELS from 2007 to 2009 and the Technical Chair of the 39th IEEE Power Electronics Specialists Conference, 2008, Rhodes, Greece.



Georgios D. Demetriadis (M'06) was born in Famagusta Cyprus. He received the M.Sc. degree (1992) in electrical engineering from the Democritus University of Thrace in Greece, his Technical Licentiate degree (2001) and the Ph.D. degree (2005) both in power electronics from the Royal Institute of Technology, KTH, in Stockholm, Sweden. He worked in Cyprus for a two years period and in 1995 he joined what is today known as ALSTOM Power Environmental Systems in Sweden. In the year 2000 he joined

ABB Corporate Research where he is currently working as a research and development manager. From 2013 he is a visiting associated professor in the Indian Institute of Technology, IIT Bombay, Mumbai, India. His main research interests include power electronics, VSC HVDC, FACTS devices, high-frequency DC-DC power resonant converters and high-frequency electromagnetic modelling.